

## Fabrication of SiO<sub>2</sub> glass fibres by thermoplastic extrusion

Juliane Heiber, Frank Clemens, and Thomas Graule

Eidgenössische Materialprüfungs- und Forschungsanstalt (EMPA), Dübendorf (Switzerland)

Dagmar Hülsenberg

Technische Universität Ilmenau, Ilmenau (Germany)

The fabrication of silica glass fibres by thermoplastic extrusion of nanosize and micron SiO<sub>2</sub> powders has been investigated. The powders were mixed with a binder system, compounded for 3 h at 150 °C, and finally extruded through a die with a 500 µm-diameter die land. After debinding the green fibres at 500 °C, these were sintered for 1 h at 1100 °C under air to yield glassy and crack-free silica fibres with a final diameter of 400 µm.

The effect of the two different particle size distributions as well as the influence of varying powder loading (between 38 and 58 vol.%) on the rheological properties of the feedstocks were analysed using capillary rheometry. The debinding and sintering behaviour was also investigated using mercury intrusion porosimetry, thermal gravimetric analysis and dilatometry.

### 1. Introduction

Today a variety of possibilities are available to produce silica glass fibres: melting [1] and drawing technologies [2 and 3] as well as technologies based on sol-gel processing [4 and 5]. Conventional melting and drawing techniques require high processing temperatures ( $\geq 1700$  °C) [6]. Furthermore, the preparation of high-purity silica glass by melting is restricted due to processing temperatures on the order of 1900 °C which cause impurities to be absorbed from the refractories in the glass melter [7]. Fibres obtained by the sol-gel process are handicapped by an inherently high densification shrinkage.

Clasen [8] showed an alternative method for the fabrication of silica glass fibres which is based on the ceramic powder route. High-purity silica glass rods were prepared by extruding a mixture consisting of 55 to 65 wt% (35 to 45 vol.%) Aerosil OX 50 in an aqueous-based binder. One disadvantage of such a binder system is that at higher pressures the solvent and binder may separate from the powder. In order to avoid this problem, a thermoplastic binder system was used in the current study to develop SiO<sub>2</sub> glass fibres.

### 2. Experimental procedure

#### 2.1 Raw materials

Based on the work of Clasen [9], nanosized fumed silica powder Aerosil OX 50 (Degussa AG) was chosen for this

Received 8 December 2003, revised manuscript 23 June 2004.

Presented in German at: 77<sup>th</sup> Annual Meeting of the German Society of Glass Technology (DGG) in Leipzig on 28 May 2003.

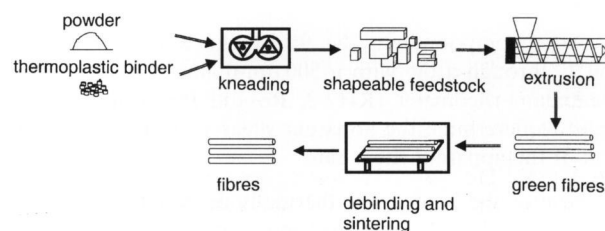


Figure 1. SiO<sub>2</sub> fibre processing by the powder extrusion technique [10].

study. For comparison of the mixing, rheological and debinding behaviour, a submicron SiO<sub>2</sub> powder S2046 (Cerac, Inc.) was also studied in parallel. Both powders were characterized by measuring the particle size distribution and the specific surface area by laser diffraction particle size analysis (LS230, Beckman Coulter) and the BET method (Coulter<sup>®</sup> SA3100<sup>TM</sup>, Beckman Coulter), respectively.

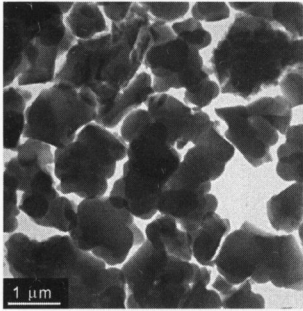
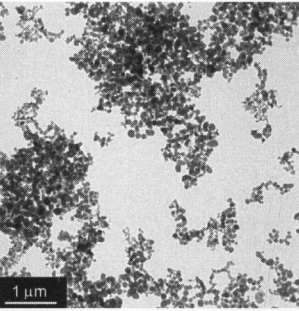
The thermoplastic binder system used was a mixture of polyethylene (Lacqtene, elf atochem S.A.) and wax (Licomont, Clariant GmbH). The decomposition behaviour was investigated by thermal gravimetric analysis (TGA, Netzsch STA 409, Netzsch Gerätebau GmbH).

#### 2.2 Fibre processing

The fibre processing method is shown schematically in figure 1. The SiO<sub>2</sub> powders and the binder components were first mixed in a high-shear mixer (Rheomix 600, Thermo Haake, Gebrüder Haake GmbH) with roller-blades at 150 °C for 3 h to yield a homogeneous feedstock. During the compounding process the torque was recorded.

Table 1. Physical characteristics of the silica powders (particle size distribution given by  $d_{10}$ ,  $d_{50}$  and  $d_{90}$ , specific surface area characterized by  $S_A$  and  $d_{BET}$ , and the agglomeration factor  $d_{50}/d_{BET}$ )

S2046		OX 50	
$d_{10}$	= 0.38 $\mu\text{m}$	$d_{10}$	= 0.07 $\mu\text{m}$
$d_{50}$	= 1.60 $\mu\text{m}$	$d_{50}$	= 0.11 $\mu\text{m}$
$d_{90}$	= 3.38 $\mu\text{m}$	$d_{90}$	= 0.21 $\mu\text{m}$
$S_A$	= 3 $\text{m}^2/\text{g}$	$S_A$	= 55 $\text{m}^2/\text{g}$
$d_{BET}$	= 0.96 $\mu\text{m}$	$d_{BET}$	= 0.05 $\mu\text{m}$
$d_{50}/d_{BET}$	= 1.7	$d_{50}/d_{BET}$	= 2.2

At this process stage, the influence of varying powder loadings (38 to 58 vol.%) and changing ratios of polyethylene (PE) to Licomont wax (1:9; 1:1; 9:1; 10:0) was investigated.

After compounding, the feedstocks were extruded at 150 °C through a die with a 500  $\mu\text{m}$ -diameter orifice using a capillary rheometer (RH7-2, Rosand Precision Ltd.) in order to determine the apparent shear viscosity as a function of the apparent shear rate.

Finally, the binder was thermally debound at temperatures up to 500 °C and the fibres sintered at 1100 and 1200 °C for 2 h. The pore size distribution prior to sintering was measured by mercury intrusion porosimetry (MIP) (CE Pascal 140/440, ThermoQuest) and the crystallization behaviour during sintering was characterized using dilatometry (DIL802, Bähr Thermoanalyse GmbH).

### 3. Results and discussion

#### 3.1 Raw materials characterization

##### 3.1.1 $\text{SiO}_2$ powder

The particle size distributions and the specific surface areas ( $S_A$ ) measured for the two powders are shown in table 1.

The fumed silica powder OX 50 has an average particle size  $d_{50}$  of 110 nm whereas the average particle size of the S2046 powder is around ten times higher ( $d_{50} = 1.6 \mu\text{m}$ ). An obstacle to obtaining homogeneous ceramic/powder mixtures is the presence of powder agglomerates which must be destroyed during the mixing process. Because of this, an important powder characteristic for the homogenization during mixing is the agglomeration factor  $Z$  which describes the ratio between the measured average particle size  $d_{50}$  (which includes agglomerates) and the average particle size  $d_{BET}$  (indicative of the primary particle size) which, in turn,

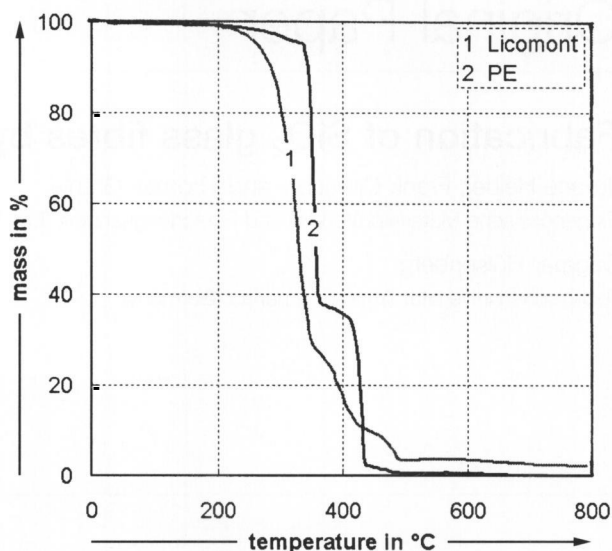


Figure 2. Mass loss of the binder components as a function of temperature.

is calculated from the specific surface area  $S_A$  and the density  $\rho$ .

The corresponding equations are shown below:

$$Z = \frac{d_{50}}{d_{BET}}, \quad (1)$$

$$d_{BET} = \frac{6}{\rho \cdot S_A}. \quad (2)$$

In equation (2), the assumption is made that the particles are spherical.

In both raw materials the agglomeration factor is around 2, which shows that the powders are not significantly agglomerated and that obtaining homogeneous mixtures should be possible.

The TEM pictures in table 1 give a visual impression of the two powders and confirm the measured values.

##### 3.1.2 Binder

Figure 2 shows the results of the thermal gravimetric analysis of the two binder components PE and Licomont.

At 220 °C, both components start to decompose. At 350 and 420 °C, PE exhibits two abrupt mass loss steps of 60 and 30 wt%, respectively, and at 500 °C it is completely pyrolyzed. Thus, during debinding, the heating rate must be kept low to prevent cracks forming and dwell times are necessary at 350 and 420 °C. In comparison to PE, the Licomont wax experiences its main mass loss of 65 wt% in a wider temperature range (between 280 to 350 °C). Above 350 °C the decomposition slows down and ends at 500 °C. At this temperature the material is not pyrolyzed completely, and the data indicates that nearly four percent of organic residues, in the form of carbon, for example, could remain in the fibres.

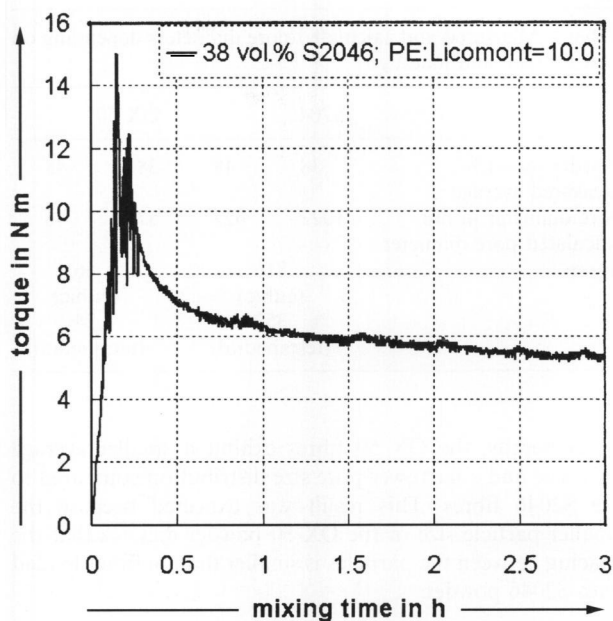


Figure 3. Torque as a function of time during compounding.

## 3.2 Feedstock preparation and characterization

### 3.2.1 S2046 powder

Torque evolution during the three hour compounding process is explained on the basis of figure 3.

During the first 10 min, the torque increase is caused by adding powder into the mixing chamber containing the melted binder components. The torque initially increases because until they are mixed with binder, the ceramic powder particles cannot flow easily past one another and along the mixer walls. Furthermore, adding the powder causes the temperature of the mixture to decrease which in turn causes the viscosity of the binder to increase. Once the powder particles have been fully heated up and coated with binder, the torque decreases until the particles are deagglomerated and the feedstock is homogenized.

In figure 4, the average torque of the last 30 min of compounding and the apparent shear viscosity for an apparent shear of  $1000 \text{ s}^{-1}$  as a function of the PE : Licomont ratio are shown (dashed lines for S2046).

In general, the torque and the apparent shear viscosity increase with increasing PE content. This behaviour was expected because Licomont is a wax with a lower viscosity compared to PE. Additionally, rheological analysis showed that the mixture exhibits shear thinning behaviour, i.e. with increasing shear rate, the apparent shear viscosity decreases [11]. This property is highly desirable for the extrusion of fibres, rods or tubes because under the high-shear conditions in the extrusion die, the mixture flows with little resistance and upon leaving the die into free space (shear rate drops to zero) the extrudate becomes rigid and retains its shape [12].

Further investigations were done on feedstocks with powder loadings higher than the 38 vol.% above because high green densities aid densification and reduce shrinkage during sintering. Because a low shear viscosity is beneficial for extrusion, these investigations were done with the binder

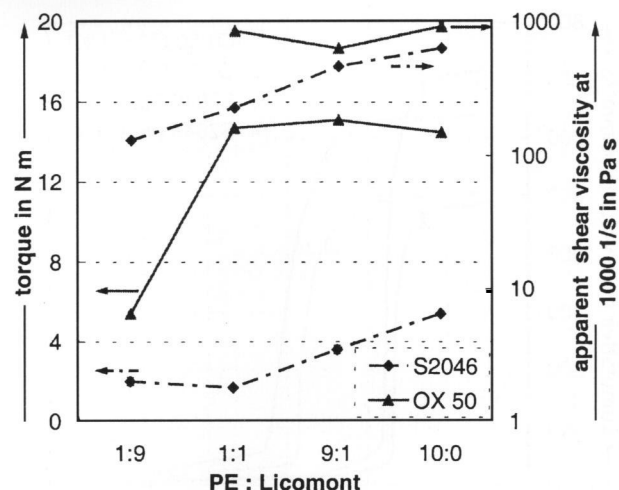


Figure 4. Torque and apparent shear viscosity as a function of binder composition for the 38 vol.% S2046 and OX 50 feedstocks.

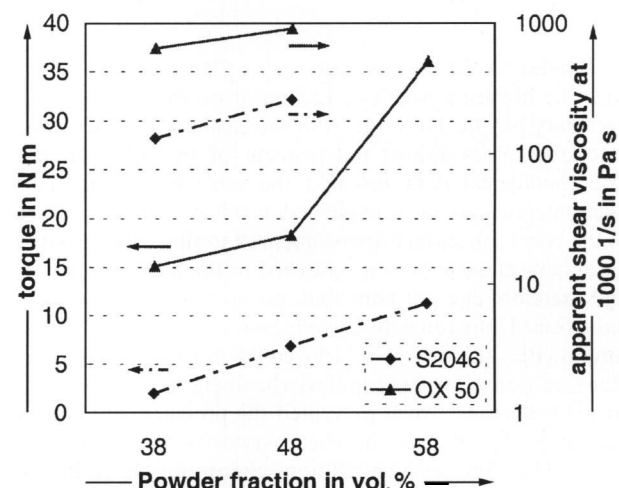


Figure 5. Torque and apparent shear viscosity as a function of S2046 and OX 50 powder loading.

system containing the highest amount of wax (PE : Licomont = 1:9). The results are shown in figure 5 (dashed lines).

As the amount of powder increases, more binder is used to wet the increased particle surface area, and therefore the part of binder which contributes to flow is reduced. As a result, the torque and the viscosity rise. The feedstock with 58 vol.% SiO<sub>2</sub> powder could not be rheologically characterized because the force necessary to cause the material to flow through the die exceeded the equipment limit.

### 3.2.2 OX 50 powder

Experiments using the same parameters as above were also done for feedstocks loaded with OX 50. For feedstocks containing 38 vol.% OX 50, the torque and the apparent shear viscosity depending on the binder composition are shown in figure 4 (solid lines for OX 50).

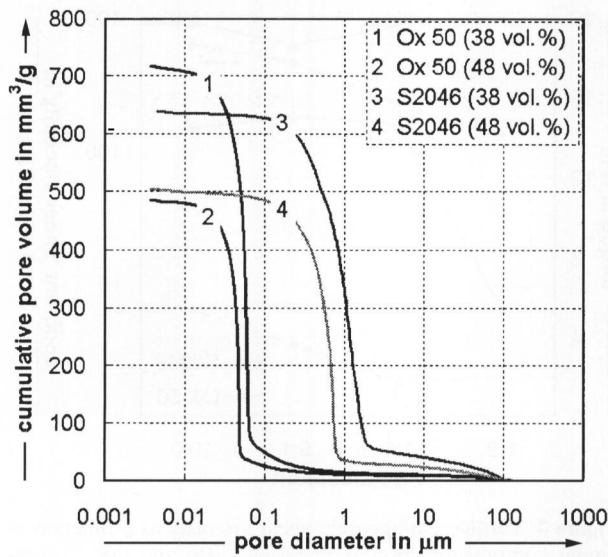


Figure 6. Pore size distribution after presintering at 500°C as a function of powder type and powder loading in the green fibre.

Similar to the results above with S2046, the feedstock with the highest amount of Licomont exhibited the lowest necessary torque. However, with increasing PE content, the torque becomes almost independent of the wax content. The rheological data revealed the same behaviour. This phenomenon cannot be explained at this point, but because of the very high surface area compared to the S2046 powder, we assume that the wax is adsorbed to the particle surfaces and therefore can not contribute to the torque or viscosity reduction. Unfortunately, the material exhibiting the lowest torque (PE : Licomont = 1:9) could not be rheologically characterized using the capillary rheometer because of slip-stick<sup>2)</sup> behaviour, which prevented the pressure equilibrium necessary to calculate the shear viscosity from being reached. Thus, further investigations concerning the influence of powder loading were done with the binder system consisting of PE : Licomont = 9:1 (figure 5 – solid lines).

Similar to the S2046 feedstock series (figure 5 – dashed lines), the torque and the apparent shear viscosity rise with increasing OX 50 powder loading and the 58 vol.% feedstock could not be rheologically characterized because the force necessary exceeded the hardware limits.

### 3.3 Debinding and sintering

#### 3.3.1 Debinding

After debinding, open porosity with a narrow pore size distribution is required for successful sintering [13]. In order to check the pore space development in the samples, pore size distributions were measured on fibres debound at 500°C using mercury intrusion porosimetry (MIP). Figure 6 shows the cumulative pore volume as a function of the pore diameter for fibres consisting of S2046 and OX 50.

<sup>2)</sup> Extrudate flow accompanied by steadily decreasing pressure, followed by a momentary halt in flow and increasing pressure up to some threshold value where flow recommences.

Table 2. Measured and calculated pore diameters depending on powder type and loading

	S2046		OX 50	
powder in vol.%	38	48	38	48
measured average pore diameter in nm	1022	623	57	46
calculated pore diameter in nm	816 (cubic) 352 (tetrahedral)		56 (cubic) 24 (tetrahedral)	

Generally, the OX 50 fibres exhibit a smaller average pore size and a narrower pore size distribution compared to the S2046 fibres. This result was expected because the smaller particle size of the OX 50 powder dictates that the spacing between the particles is smaller than in fibres loaded with S2046 powder.

It is also evident that with increased powder loadings the average pore size and the cumulative pore volume decrease both for S2046 and OX 50. The reduced average pore size is caused by closer packing of the particles which translates directly into a smaller interparticle separation. The total volume of pores decreases because less volume is occupied by binder which generates the pores upon decomposition. Thus, the cumulative pore volume should be constant for a defined binder content independent of the kind of powder. The difference in cumulative pore volume between the fibres loaded with 38 vol.% S2046 and those with 38 vol.% OX 50 may be a consequence of the fragility of the debound S2046 fibres. We suspect that during filling the sample container with mercury, the S2046 fibres were partially crushed and that a certain fraction of the larger pore consequently collapsed and were not registered by the analysis.

After Reed [14], the average pore size can be estimated. According to this reference, the cross-sectional pore area *A* is a function of both the average size of the spherical particles *d*<sub>50</sub> (table 1), and the packing arrangement (equations (3 and 4)).

$$\text{cubic packing: } A = 0.21 \cdot d_{50}^2, \quad (3)$$

$$\text{tetrahedral packing: } A = 0.04 \cdot d_{50}^2. \quad (4)$$

Under the assumption of spherical pores, the pore diameter, *d*, is approximated by equations (5 and 6):

$$\text{cubic packing: } d = \sqrt[2]{\frac{0.21}{\pi}} d_{50}, \quad (5)$$

$$\text{tetrahedral packing: } d = \sqrt[2]{\frac{0.04}{\pi}} d_{50}. \quad (6)$$

The measured and the calculated pore diameters are listed in table 2.

Comparing the theoretical and measured values for the OX 50 38 vol.% green fibres, it appears that these possess cubic packing and that with increasing powder loading the

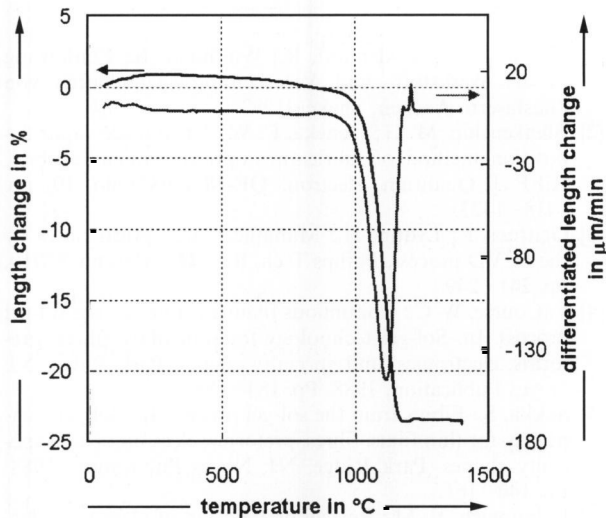


Figure 7. Relative length change as a function of temperature for an OX 50 rod.

packing density shifts towards tetrahedral packing. In contrast, the measured average pore diameter of the 38 vol.% S2046 debound fibres is greater than expected from equation (5) for cubic packing, indicating that cubic packing is not reached. Only upon increasing the powder loading does the packing improve and begin to approach tetrahedral packing.

Further investigations showed that the pore size distribution is independent of the composition of the binder system, and that there was no densification up to 900°C.

Scanning electron microscopy investigations showed that green fibres consisting of 38 vol.% OX 50 powder and a PE : Licomont ratio of 9:1 exhibited cracks along the fibre axis after debinding. The frequency and size of the cracks decreased with increased powder loadings, and no cracks occurred at higher Licomont concentrations. Thermal gravimetric analysis (figure 2) showed that Licomont decomposes in a wider temperature range than PE and we assume that because of the abrupt decomposition of PE and the small average pore size, a rapid build-up of pressure in the fibres caused the cracks to form. For binder burnout of fibres loaded with S2046, the larger pores in this material eased the transport of decomposition products, allowing crack-free fibres to be achieved independent of the PE : Licomont ratio.

### 3.3.2 Sintering

Dilatometry measurements on rods consisting of OX 50 were performed to determine the optimal sintering temperature (figure 7).

Densification starts at 950°C and reaches a maximum at 1120°C. At temperatures above 1200°C a second peak occurs which was assumed to be related to a crystallization event. To check this hypothesis, two rods sintered at maximum temperatures of 1100 and 1400°C were also characterized by dilatometry (figure 8). The rod sintered at 1100°C showed a monotonically rising expansion curve with increasing temperature. In contrast, the characteristic of the

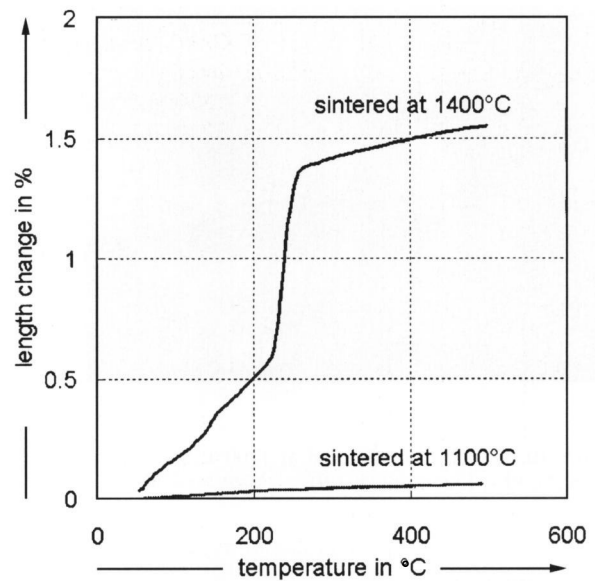


Figure 8. Relative length change as a function of temperature for two OX 50 rods sintered at different temperatures.

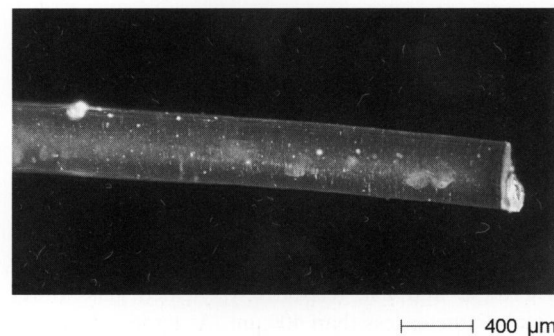


Figure 9. OX 50 fibre sintered at 1100°C for 2 h (feedstock: 48 vol.%; PE : Licomont = 1:9).

rod sintered at 1400°C exhibited discontinuities at 150 and at 235°C which can be correlated with the transitions from low to high tridymite and from low to high cristobalite, respectively. Since in high-purity SiO<sub>2</sub> tridymite should not occur [15], the starting powder must have been contaminated during processing (e.g. equipment wear, binder residues). Figure 9 confirms that OX 50 fibres sintered at 1100°C for 2 h are glassy and crack-free while OX 50 fibres sintered at 1200°C for 2 h exhibit numerous cracks on the surface (figure 10) associated with the volume change upon crystallization.

Debound S2046 fibres could not be sintered successfully. Shrinkage measurements showed that densification did not run to completion below 1300°C, and that at higher sintering temperatures crystallization occurred. Because of the coarser particles in the S2046 powder, the sintering activity was too low and consequently dense and glassy fibres could not be achieved.

## 4. Conclusion

One submicron and one nanosized silica powder were used to investigate the fabrication of silica glass fibres via ex-

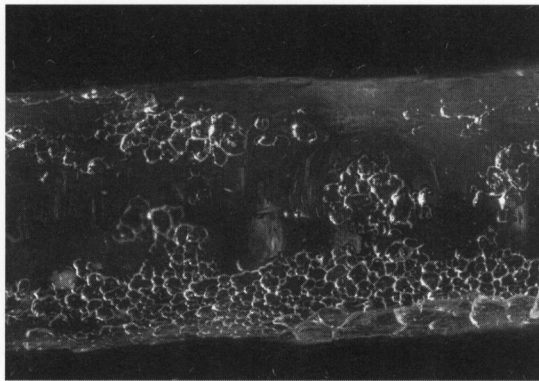


Figure 10. OX 50 fibre sintered at 1200°C for 2 h (feedstock: 48 vol.%; PE : Licomont = 1:9).

trusion. While the feedstocks composed of the relatively coarse submicron powder showed better rheological properties (lower torque and shear viscosity), only the fibres consisting of nanosized particles could be successfully densified to crack-free silica glass fibres.

For the fibres made of nanosized particles, the best rheological properties are obtained with the binder system consisting of PE : Licomont = 9:1, however, only the green fibres formed with PE : Licomont = 1:9 could be debound crack-free. The maximum powder loading achieved during mixing was 58 vol.%, but this feedstock could not be extruded, thus 48 vol.% OX 50 powder was considered to be the maximum useful loading. A sintering temperature and time of 1100°C and 2 h, respectively, yielded glass fibres with a final diameter less than 400 µm. At temperatures exceeding 1200°C, the material crystallized and formed cristobalite.

\*

These investigations are part of the Disappearing Computer (DC) IST European Research Program (IST-200-25247). The Swiss contribution to the project is financed by the BBW (Office for Education and Science, Switzerland) under Project No. 00.0500.

#### Contact:

Juliane Heiber  
EMPA Dübendorf  
Überlandstraße 129  
CH-8600 Dübendorf  
E-mail: Juliane.Heiber@empa.ch

#### 5. References

- [1] Hörsting, K.; Kaldenhoff, R.; Wulfhorst, B.: Einführung in die Werkstoff- und Verarbeitungseigenschaften von Glasfasern. Aachen: Shaker, 1993.
- [2] Blankenship, M. G.; Deneka, C. W.: The outside vapor deposition method of fabricating optical waveguide fibres. *IEEE J. Quantum Electron.* **QE-18** (1982) no. 10, pp. 1418–1423.
- [3] Geittner, P.; Lydtin, H.: Manufacturing optical fibres by the PCVD process. *Philips Tech. Rev.* **44** (1989) no. 8/9/10, pp. 241–249.
- [4] LaCourse, W. C.: Continuous filament fibres by the sol-gel process. In: *Sol-gel technology for thin films, fibres, preforms, electronics, and specialty shapes*. Park Ridge, NJ: Noyes Publication, 1988. Pp. 184–198.
- [5] Sakka, S.: Fibres from the sol-gel process. In: *Sol-gel technology for thin films, fibres, preforms, electronics, and specialty shapes*. Park Ridge, NJ: Noyes Publication, 1988. Pp. 140–161.
- [6] Rabinovich, E. M.: Review preparation of glass by sintering. *J. Mat. Sci.* **20** (1985) pp. 4259–4297.
- [7] Brinker, C. J.; Scherer, W. G.: *Sol-gel science: the physics and chemistry of sol-gel processing*. London: Academic Press, 1990.
- [8] Clasen, R.: Preparation of high-purity silica glasses by sintering of colloidal particles. *Glastech. Ber.* **60** (1987) no. 4, pp. 125–132.
- [9] Clasen, R.: Preparation and sintering of high-density green bodies to high-purity silica glasses. *J. Non-Cryst. Solids* **89** (1987) pp. 335–344.
- [10] Clemens, F.; Buchser, W.; Graule, T.: Silicon carbide fibre extrusion – Manufacturing and tensile strength of fine sintered SiC-fibres. In: *Proc. Tenth International Ceramics Congress and the Third Forum on New Materials (CIMTEC), Florence (Italy) 2002*. Part K: Forum on New Materials – Part 5. Pp. 39–46.
- [11] Kulicke, W.-M.: *Fließverhalten von Stoffen und Stoffgemischen*. Basel: Hüthig & Wepf, 1986.
- [12] Wegmann, M. R.: *Microextrusion of barium titanate for PTCR applications*. University of Strathclyde, Glasgow, PhD thesis 2002.
- [13] Clasen, R.: *Herstellung sehr reiner Kieselgläser durch Sintern submikroskopischer Glasteilchen*. Rheinisch-Westfälische Technische Hochschule, Aachen, habilitation 1989.
- [14] Reed, J. S.: *Principles of ceramics processing*. New York: Wiley, 1995.
- [15] Schatt, W.; Worch, H.: *Werkstoffwissenschaft*. Stuttgart: Deutscher Verlag für Grundstoffindustrie, 1996.
- [16] Clemens, F.; Wegmann, M.; Graule, T. et al.: Computing fibers – a novel fiber for intelligent fabrics. *Adv. Eng. Mater.* **5** (2003) no. 9, pp. 682–687.

■ E504P002